Reac Kinet Mech Cat (2012) 105:317–334
DOI 10.1007/s11144-011-0384-2

Theoretical study of the interaction of simple molecules such as H_2, C_2H_2, and C_2H_4 with Pd–Pb catalysts

Piotr Matczak

Received: 13 May 2011 / Accepted: 1 October 2011 / Published online: 21 October 2011

Abstract A study of the interaction between some simple molecules (dihydrogen, acetylene, and ethylene) and Pd–Pb catalysts has been performed using the B3LYP hybrid density functional. The reaction paths for the H_2 molecule reacting with the PdPb dimer are reported for the singlet and triplet spin states. The C_2H_2 and C_2H_4 molecules were adsorbed in a few characteristic sites on the Pd(100) surface doped with Pb. This surface was modeled using $Pd_{13}Pb$ clusters. The results of the calculations indicate that the Pd–Pb catalysts interact with the H_2, C_2H_2, and C_2H_4 molecules more weakly than the corresponding monometallic Pd catalysts do, and thus the bimetallic catalysts exhibit the reduced activity toward these simple molecules.

Keywords Hydrogen molecule · Acetylene adsorption · Ethylene adsorption · Pd–Pb catalyst · DFT

Introduction

Palladium is widely used as a catalyst of selective hydrogenation reactions [1–3]. The selective hydrogenation of alkynes to mono-olefins, that is, the so-called semihydrogenation of alkynes, is a crucial step in many laboratory and industrial processes [2]. In particular, the semihydrogenation of acetylene to ethylene is required in the production of polyethylene [4, 5]. In the polymerization of C_2H_4, the

Electronic supplementary material The online version of this article (doi: 10.1007/s11144-011-0384-2) contains supplementary material, which is available to authorized users.

P. Matczak (✉)
Department of Theoretical and Structural Chemistry, University of Łódź,
Pomorska 165, 90-236 Lodz, Poland
e-mail: p.a.matczak@gmail.com

complete elimination of C_2H_2 from ethylene feedstocks via the semihydrogenation is to avoid deactivation of polymerization catalysts.

According to the classical interpretation, the high selectivity of Pd toward the semihydrogenation of alkynes is attributed to the stronger adsorption of alkynes on the Pd surface compared to that of alkenes formed in the semihydrogenation reaction [2]. Since the interaction between alkynes and the catalyst surface is thermodynamically preferred, the formed alkenes are displaced from the surface and their readsorption is blocked. As a consequence, alkynes are hydrogenated to alkenes and the parallel undesirable hydrogenation of alkenes to alkanes is suppressed. It should be noted that recently the interpretation of the high selectivity of Pd has been revisited by Teschner et al. [6, 7] who have related the selectivity to the formation of a Pd/C phase on the catalyst surface. Carbon in the Pd/C phase hinders the participation of bulk-dissolved and subsurface hydrogen in the hydrogenation of alkynes [6–9]. This hydrogen is thought to be very reactive and unselective. Then alkynes are hydrogenated selectively to alkenes only by hydrogen present on the catalyst surface.

The selectivity of the Pd catalyst can be enhanced by introducing a second metal, that is, by alloying Pd with other metal, and in this manner a bimetallic catalyst is formed [10, 11]. The improvement in the catalytic selectivity has been reported for Pd mixed with various metals, e.g. with Ag [12], Au [13], Sn [14, 15], and Pb [14, 16, 17].

The interaction between C_2H_2 or C_2H_4 and the low Miller index surfaces of Pd has motivated many experimental [18–29] and theoretical [30–39] investigations aiming to understand the kinetics and the mechanism of the semihydrogenation reaction. By contrast, the adsorption of C_2H_2 or C_2H_4 on single-crystal surfaces of various bimetallic Pd–Pb catalysts has attracted much less interest, although the Lindlar catalyst, Pd–Pb/$CaCO_3$, has been known since the 1950s [40]. Furthermore, theoretical studies of the adsorption on such catalysts are very scarce. Ferullo et al. [41] have carried out semiempirical calculations for the adsorption of C_2H_2 on $Pd_3Pb(111)$ and their calculations indicate a strong negative effect of Pb atoms on the strength of the C_2H_2 adsorption on the alloy. Very recently, a periodic slab density functional theory (DFT) study has been reported by García-Mota et al. [42] and it has provided the description of the C_2H_2 and C_2H_4 adsorption on the PdPb(111) surface which was formed by the substitution of Pd atoms by Pb ones yielding the Pb amount of 0.25 ML. For both adsorbates, their adsorption energies on PdPb(111) are reduced by ca. 12–15 kcal/mol compared to the adsorption energies on Pd(111), that is, −41.05 and −18.91 kcal/mol for acetylene and ethylene, respectively [42]. A decrease of C_2H_4 adsorption energy toward less exoenergetic values has also been predicted by DFT for Pd surfaces alloyed with other second metals: PdAg(111) [38, 43], Pd/Au(111) [36], and PdSn(111) [44].

The present work is aimed at theoretical investigations of the interaction between some simple molecules (H_2, C_2H_2, and C_2H_4) and Pd–Pb catalysts. Reaction paths for the H_2 molecule on the PdPb bimetallic dimer were determined and they include such types of interaction as adsorption and dissociation of H_2, as well as absorption of the formed H atoms inside the dimer. As for C_2H_2 and C_2H_4, their adsorption on the Pd(100) surface doped with Pb was studied for various adsorption sites on this

surface to detect the most favorable one. The choice of two different Pd–Pb catalysts, that is, the bimetallic dimer and the doped surface, was dictated by the differences in the computational cost and in the number of calculations required to determine the reaction paths versus the preferred adsorption sites. The shared aspect of the above-mentioned objectives is to establish an influence of the second metal (i.e., the Pb dopant) on the interaction between the simple molecules and the Pd–Pb catalysts. For this reason, a comparison of this interaction with that on monometallic Pd catalysts is also presented.

Method

Quantum chemical calculations were conducted using DFT as implemented in the Gaussian 03 suite of programs [45]. The chosen DFT method, namely the hybrid B3LYP density functional [46], combines the exact HF exchange, the Slater local exchange functional [47], and the Becke 1988 nonlocal gradient correction to the exchange functional [48] with the correlation provided by the Vosko-Wilk-Nusair local [49] and Lee–Yang–Parr nonlocal [50] functionals. The B3LYP functional was previously applied to the investigations of the interaction between catalysts containing Pd and the H_2 and C_2H_4 molecules [32, 44, 51]. In addition, the results of some simple tests carried out for the selected systems studied in the present work proved the reliability of this functional (see Sect. S1 in the Supplemetary material). The Los Alamos relativistic effective core pseudopotentials (RECP) together with the corresponding valence basis sets in the completely uncontracted scheme (LANL08) [52, 53] were assigned to the Pd and Pb atoms. The H and C atoms were treated with the 6-311++G** basis set [54].

Reaction paths for the H_2 molecule on the PdPb dimer were determined using a routine computational procedure. A large series of geometries of the bimetallic dimer interacting with the molecular or dissociated H_2 was optimized to find stationary points, that is, all possible minima and transition states. The identification of stationary point nature was carried out with the help of vibrational frequency analysis. A stationary point was considered to be a minimum when it possessed no imaginary vibrational frequencies, whereas that with one imaginary vibrational frequency corresponded to a transition state. The intrinsic reaction coordinate (IRC) approach [55] was done with the objective of determining which of the minima are connected by a given transition state.

The interaction of the C_2H_2 and C_2H_4 molecules with the (100) surfaces of palladium and palladium doped with lead was investigated using a cluster model approach. The surfaces were modeled by 14-atom clusters that comprised three layers having 9, 4, and 1 metal atoms, respectively. The size of the clusters was chosen mainly due to the cluster symmetry and low computational cost. Nevertheless, this size makes it possible to predict some properties of bulk Pd quite accurately (see Sect. S1 in the Supplementary material) and seems to be sufficient for qualitative investigations of adsorbates on surfaces; it is worth mentioning that even smaller cluster approaches of (100) surfaces proved to be useful [32, 56]. The bimetallic clusters were formed by replacing a single surface

(i.e. from the 9-atom layer) or subsurface (i.e. from the 4-atom layer) Pd atom by the Pb one. Both Pd_{14} and $Pd_{13}Pb$ exhibit the distance from the nearest neighbor equal to the value of the Pd bulk, namely 2.7512 Å. The C_2H_2 and C_2H_4 molecules are adsorbed in three characteristic sites on the Pd(100) surface, that is, atop, bridge, and hollow (see Fig. 1). In the case of the bimetallic clusters, the picture of adsorption is slightly more complicated, since the second metal atom may be placed in the surface or subsurface layer. For this reason, the author draws a distinction of each of the three adsorption sites between two variants depending on the location of the Pb atom. An adsorption site that either contains or is adjacent to the surface Pb atom is denoted by the suffix I, whereas a site that has in its immediate proximity the subsurface Pb atom is marked with the suffix II (see Fig. 2 for graphical presentations of all six adsorption sites). In the course of the optimizations of C_2H_2 and C_2H_4 in the adsorption sites, the Pd_{14} and $Pd_{13}Pb$ clusters were assumed to keep a fixed crystal structure [32, 56]. This assumption is a crude approximation of surface phenomena but its use was necessary to force the metal clusters to mimic the symmetry of the (100) surface in the course of the adsorbate optimizations in the adsorption sites (with no constraints imposed on the geometry, the clusters evolved into isolated gas-phase structures and the adsorbate migrated round the clusters to the regions that did not represent the (100) surface).

The energy levels of the 14-atom metal clusters served as the basis for the calculations of the density of states (DOS) [57] for the Pd(100) and PdPb(100) surfaces. The energy levels and the Mulliken overlap populations of the clusters with the adsorbates were employed to determine the crystal orbital overlap population (COOP) [58]. DOS and COOP spectra were plotted using Gaussian curves with the full width at half-minimum arbitrarily equal to 6.92 kcal/mol. The calculations of DOS and COOP were carried out in the GaussSum program [59].

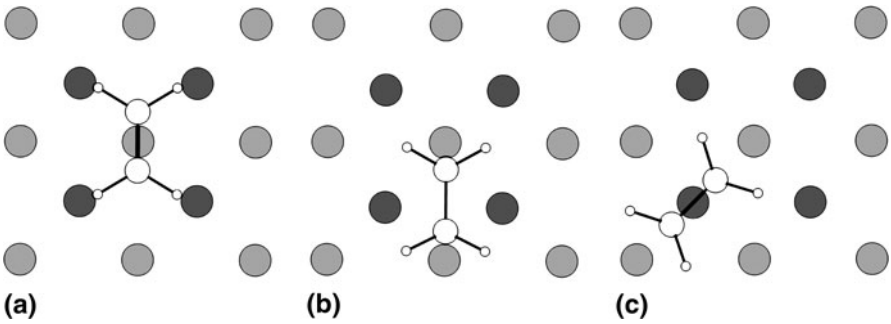

Fig. 1 Top views of the cluster representing the (100) surface with the adsorbate molecule bound in the atop (**a**), bridge (**b**), and hollow (**c**) sites. The ethylene molecule adsorbed on the Pd_{14} cluster is shown as an example. Carbon atoms are denoted by *big white circles*, hydrogen atoms by *small white circles*, and palladium atoms are *colored gray* (the first layer) and *dark gray* (the second layer). The only Pd atom from the third layer is not visible

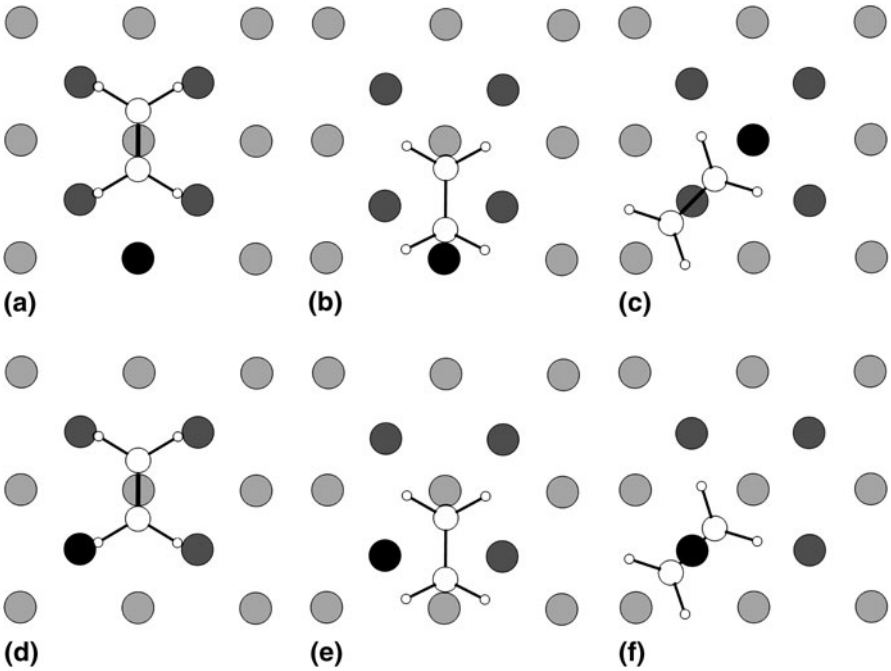

Fig. 2 Top views of the clusters representing the PdPb(100) surface with the adsorbate molecule bound in the atop-I (**a**), bridge-I (**b**), hollow-I (**c**), top-II (**d**), bridge-II (**e**), and hollow-II (**f**) sites. The ethylene molecule adsorbed on the $Pd_{13}Pb$ clusters is shown as an example. Carbon atoms are denoted by *big white circles*, hydrogen atoms by *small white circles*, and palladium atoms are *colored gray* (the first layer) and *dark gray* (the second layer). The Pb atom is marked with *black circle* regardless of its location [in the surface layer for (**a**)–(**c**) or in the subsurface layer for (**d**)–(**f**)]. The only Pd atom from the third layer is not visible

Results and discussion

Reaction paths for H_2 on PdPb

Since the energies of minima and transition states along the reaction paths are referenced to the energy of the separated H_2 and PdPb, it is necessary to determine the electronic ground states of H_2 and PdPb. The ground state of the H_2 molecule is obviously a $^1\Sigma_g^+$ state and for this state some fundamental molecular properties such as bond length, r_e, dissociation energy, D_0, and vibrational frequency, ω_e, calculated at the B3LYP/6-311++G** level of theory are shown in Table 1. The value of D_0 includes a basis-set superposition error (BSSE) correction [63] and the zero-point vibrational energy (ZPVE). The calculated values of all three properties are very close to the experiment [60]. In the case of the PdPb dimer, its ground state is predicted to be a $^1\Sigma$ state. The molecular properties of this dimer are also listed in Table 1. Similarly to H_2, the D_0 value of PdPb incorporates a BSSE correction and the ZPVE. The values of PdPb properties obtained by means of B3LYP/LANL08 can be compared with the results of relativistic four-component DFT calculations

Table 1 Comparison of the calculated bond length, r_e, dissociation energy, D_0, and vibrational frequency, ω_e, of H_2 and PdPb with available theoretical and experimental findings

Molecule/method	r_e (Å)	D_0 (kcal/mol)	ω_e (cm^{-1})
H_2			
This work	0.744	103.53	4,418.1
Experiment [60]	0.741	107.92	4,401.2
PdPb			
This work	2.450	49.24	218.2
4-comp-DFT [61]	2.5	44.97	201.8
Experiment [62]		25.81	

[61]. There are no significant differences between the results of both theoretical approaches. To our knowledge, the D_0 value of 25.81 kcal/mol [62] is the only available PdPb property estimation which is based on experimental measurements. Both theoretical results are rather far away from this experimental estimation. On the other hand, the authors of [62] stated that their value is merely a preliminary result. The presented comparison of the results calculated in the present work with the experimental (for H_2) and advanced high-level theoretical (for PdPb) data suggests that the B3LYP functional combined with the 6-311++G** and LANL08 basis sets provides a reasonable description of H_2 and PdPb and is sufficient for qualitative investigations of these molecules interacting with each other.

For the reaction of H_2 with PdPb, its paths were determined in two spin states, namely in singlet and triplet. The former turns out to be lower in energy than the latter whose all minima exhibit endoenergetic energies (with respect to the energy of the separated H_2 and PdPb in their ground states). For this reason, the triplet reaction path is not analyzed here and its graphical presentations can be found in the Supplementary material (see Figs. S1 and S2).

The geometries of the minima and transition states of H_2 interacting with PdPb along the singlet reaction path are shown in Fig. 3. The energies, E, corresponding to the minima and to the transition states are plotted in Fig. 4. The E values were corrected by the appropriate ZPVEs. Approaching the dimer by its Pd end, the H_2 molecule combines with the dimer with a very small exoenergetic effect of −0.59 kcal/mol. The H–H bond is elongated by 0.032 Å compared to the bond length in a free H_2 molecule (see Table 1), implying the molecular capture of H_2. The applied computational method predicts that the system loses its symmetry (a T-shaped minimum by the Pd end was not detected) but it remains planar. In the transition state TS1, the H_2 molecule undergoes dissociation and one of the H atoms lies out of the plane containing the remaining three atoms (the dihedral angle of 65.1°). Having crossed the TS1, the system falls into the global minimum IM1, $E = -9.93$ kcal/mol. Next, the reaction can proceed through one of two possible transition states, TS2 or TS2′. The TS2 one is accompanied by far lower energetic barrier although the Pd–Pb bond lengthens considerably (to 2.625 Å). In the minimum IM2, the system exhibits the E value only slightly less exoenergetic than that in the IM1. As opposed to the IM1, all the atoms lie in a plane. Overcoming the

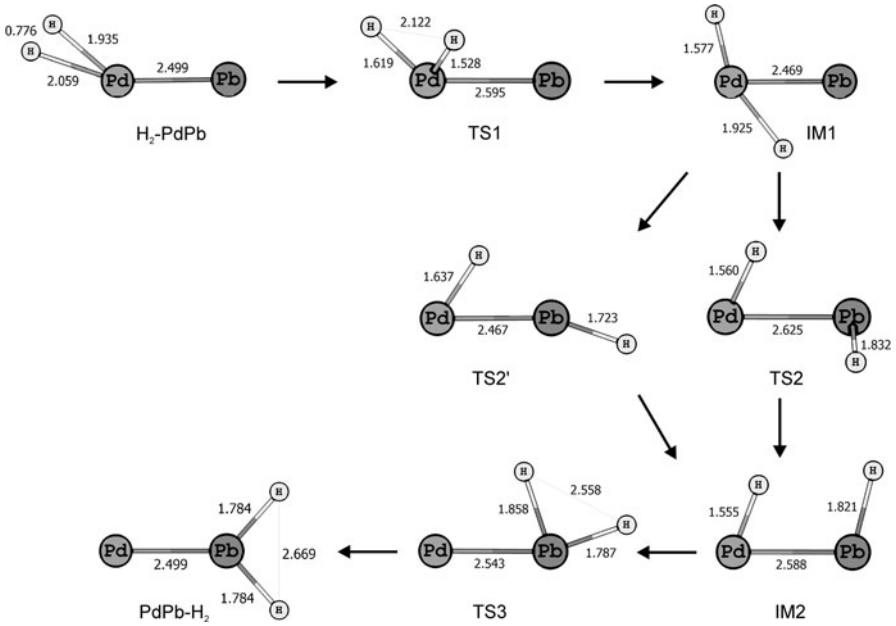

Fig. 3 Reaction path for H_2 on PdPb in the singlet spin state. The calculated bond distances (in Å) are also displayed

barrier TS3, $E = 14.31$ kcal/mol, leads the system to the structure obtained by approaching the H_2 molecule by the Pb end. The PdPb–H_2 minimum exhibits a symmetric and planar geometry. The H_2 molecule is dissociated and the H–H distance amounts to 2.669 Å. However, the E value is higher relative to the energy of the separated H_2 and PdPb.

It is desirable to comment on the presented reaction path including its catalytic aspect. The molecular capture of H_2 occurs only by the Pd end of the dimer. When the H_2 molecule approaches the Pb end, the reaction path runs solely through endoenergetic E values and directly leads to the activated dissociation of H_2 in the PdPb–H_2 minimum. These results can be interpreted in two ways. First, the exoenergetic interaction in the H_2–PdPb minimum suggests that the H_2 adsorption by the Pd end is energetically preferred. As a matter of fact, the energetic preference of the Pd end has also been observed for the interaction between the H_2 molecule and the PdCu, PdAg, and PdAu bimetallic dimers [51, 64]. It obviously results from the fact that Pd exhibits higher activity toward H_2 than the second metals in these dimers. Second, there is a mutual impact of the metals on their adsorption properties. The ability of the Pd end in the bimetallic dimer to adsorb H_2 is inferior to that of the monometallic Pd_2 dimer. Alikhani and Minot [65] calculated the energetic effect of the molecular adsorption of H_2 on Pd_2 in the T-shaped geometry and their value of -7.0 kcal/mol is much more exoenergetic than that of H_2–PdPb (-0.59 kcal/mol). It suggests that Pb poisons the H_2 adsorption ability of Pd and, therefore, reduces the catalytic activity of the PdPb dimer. The negative effect produced by Pb seems to be

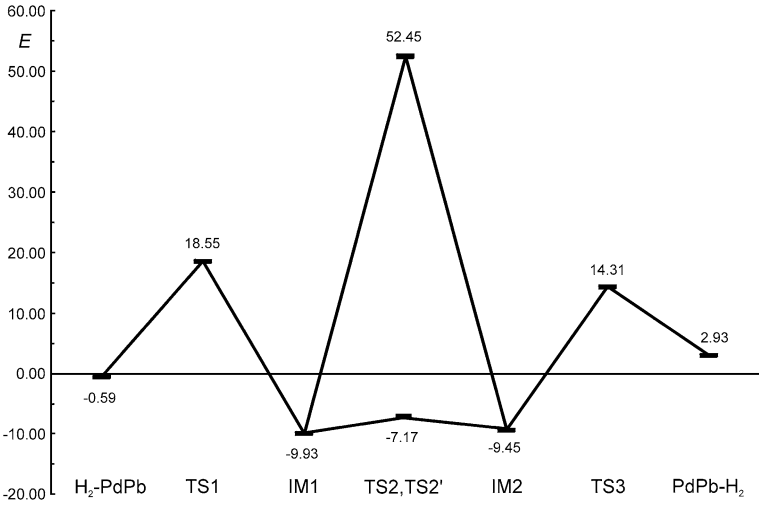

Fig. 4 Reaction path for H_2 on PdPb in the singlet spin state, with energies of the minima and of the transition states that correspond to the structures in Fig. 3. The energy, *E* (in kcal/mol), is reported with respect to the energy of the separated H_2 and PdPb in their ground states

even stronger than that of Cu, Ag, and Au [51, 64]. The existence of the barriers at the Pd and Pb ends, i.e., the TS1 and TS3, respectively, excludes spontaneous dissociation of H_2, while the H_2 dissociation on Pd_2 can proceed without activation energy [65]. Furthermore, the Pb atom also has an influence on the bonding of the dissociated H atoms with the bimetallic dimer. The *E* values in the IM1 and IM2 minima are only about one-fourth of the energetic effect observed for two H atoms bound inside the Pd_2 dimer, −38.1 kcal/mol [65]. On the other hand, Pd may promote slightly the reactivity of Pb. Obviously, the *E* value in the PdPb–H_2 minimum is endoenergetic but it is less than 3 kcal/mol, implying a relatively easy activation. Interestingly, the TS3 barrier is lower than the TS1 one.

Adsorption of acetylene on Pd(100) and PdPb(100)

The adsorption of acetylene on the Pd(100) surface has been the subject of a few experimental studies [18, 25, 29]. Acetylene adsorbs nondissociatively at room temperature on Pd(100) and its molecular geometry is strongly distorted with C-atom hybridization shifting close to sp^3 [18]. The C_2H_2 molecule is bound with the surface in a di–σ configuration, i.e., each carbon atom is attached to a Pd atom. The energetics of the C_2H_2 adsorption on Pd(100) has been investigated by Vattuone et al. [29] using single-crystal adsorption calorimetry. The initial heat of adsorption amounts to ca. −27 kcal/mol and it changes slowly in the range of C_2H_2 coverage from 0 to 0.4 ML. At steady state, it becomes considerably less exoenergetic and the measured value is equal to ca. −10 kcal/mol. The authors of [29] have suggested that the value of the initial heat of adsorption corresponds to the di–σ configuration of C_2H_2, while the steady-state one might be ascribed to a

π-bonded state (i.e., the center of C–C bond is located on top of a Pd atom). Experimental studies of the C_2H_2 adsorption on PdPb(100) have not been reported.

Table 2 summarizes the calculated energetic, structural, and electronic properties of the C_2H_2 molecule adsorbed in the characteristic sites on the Pd(100) and PdPb(100) surfaces. The energetically preferred adsorption site on Pd(100) is the hollow one, $E_{ads} = -33.92$ kcal/mol. The bridge site exhibits slightly less exoenergetic effect. In both these sites, each carbon atom of the C_2H_2 molecule is bound with a Pd atom and, therefore, these sites correspond to di–σ configurations. The geometry of the C_2H_2 molecule undergoes a significant change in the adsorption process. As it is indicated by the δ_{C-C} and δ_{C-C-H} parameters, the C–C bond is elongated and the C–C–H angles are bent upward implying a rehybridization of the C atoms from sp to sp^2. Even though the experiment predicts a stronger rehybridization ($\sim sp^3$) [18], the main conclusion concerning the deformation of di–σ-bonded C_2H_2 remains valid. Furthermore, the calculated E_{ads} values in the bridge and hollow sites are close to the experimental value of ca. -27 kcal/mol [29]. The adsorption in the atop site shows the least exenergetic effect with almost unperturbed geometry of the C_2H_2 molecule. The E_{ads} value in this site seems to be in line with the weakly π-bonded C_2H_2 hypothesis formulated by Vattuone et al. [29].

The electronic charge gathered in the C_2H_2 molecule indicates a charge transfer between the adsorbate molecule and the surface. According to the Dewar-Chatt-Duncanson model of orbital interaction [66, 67], the HOMO of the adsorbing C_2H_2 molecule can hybridize with Pd orbitals resulting in an electronic donation from the adsorbate to the surface. This transfer is accompanied by a back-donation of electronic charge from the occupied Pd orbitals to the adsorbate LUMO. In the case of C_2H_2 adsorbed in the bridge and hollow sites on Pd(100), the charge back-donation outweighs the donation, as it is illustrated by the negative values of both Mulliken population analysis [68] and natural population analysis [69] charges of the C_2H_2 molecule. For the atop site, a very small charge transfer is expected and, therefore, the Q_{NPA} value seems to be more realistic.

It is convenient to start presenting the C_2H_2 adsorption on the PdPb(100) surface with both variants of the bridge and hollow sites, since the atop sites behave differently. For each location of the second metal atom, the hollow site is energetically more favorable than the bridge one. In general, the hollow-II variant turns out to be the most favorable site on the investigated bimetallic surface. The bridge-II and hollow-II sites, that is, those with the Pb atom in the subsurface layer, are preferred to the bridge-I and hollow-I ones, that is, those with the Pb atom in the surface layer. It leads to a general observation that the closer the Pb atom is located to the adsorption site, the less exoenergetic the C_2H_2 adsorption becomes. The change of E_{ads} toward less exoenergetic values is accompanied by the increase of the height, d, of the adsorbed molecule from the surface. For the bridge and hollow sites in both variants, the back-donation of electronic charge from the surface predominates resulting in the negative values of Q_{MPA} and Q_{NPA}.

When compared with the Pd(100) surface, the bimetallic one exhibits less exoenergetic E_{ads} values and, therefore, the reduced activity toward the C_2H_2 adsorption. As a result, the Pb atom present in the adsorption sites or in their nearest

Table 2 Energetic, structural, and electronic properties of the acetylene molecule adsorbed in the characteristic sites on the Pd(100) and PdPb(100) surfaces

Surface	Site	E_{ads} (kcal/mol)[a]	d (Å)[b]	R(C–C) (Å)	R(C–H) (Å)	∠(C–C–H) (°)	δ_{C-C} (Å)[c]	δ_{C-C-H} (°)[d]	Q_{MPA} (e)[e]	Q_{NPA} (e)[e]
Pd(100)	Atop	−5.38	2.241	1.225	1.065	164.1	0.026	15.9	0.2565	−0.0395
	Bridge	−25.35	1.864	1.305	1.085[f]	133.1	0.106	46.9	−0.1391	−0.2915
					1.087	133.1		46.9		
	Hollow	−33.92	1.513	1.337	1.094	123.2	0.138	56.8	−0.2313	−0.4956
					1.095	123.2		56.8		
PdPb(100)	Atop-I	−6.14	2.120	1.243	1.068	155.8	0.044	24.2	0.0671	0.0748
	Bridge-I	−2.65	1.997	1.310	1.085	131.3	0.111	48.7	−0.4717	−0.4517
					1.090	129.7		50.3		
	Hollow-I	−8.63	1.711	1.333	1.088	123.7	0.134	56.3	−0.4903	−0.5986
					1.098	121.8		58.2		
	Atop-II	−5.14	2.263	1.220	1.066	168.2	0.021	11.8	0.1251	−0.0016
					1.066	169.1		10.9		
	Bridge-II	−21.94	1.877	1.295	1.084	134.5	0.096	45.5	−0.0839	−0.0558
					1.086	134.9		45.1		
	Hollow-II	−24.41	1.577	1.320	1.092	124.6	0.121	55.4	−0.1181	−0.4620
					1.091	126.1		53.9		

[a] The adsorption energy calculated by subtracting the energy of the separated gas-phase C_2H_2 molecule and the Pd_{14} or $Pd_{13}Pb$ cluster from the energy of the cluster with the adsorbed C_2H_2 molecule

[b] The height of the adsorbed molecule measured from the surface

[c] The elongation of the C–C bond, R, with respect to the C–C bond length in the gas phase (see Table S1 in the Supplementary material)

[d] The change of the C–C–H angle, ∠, with respect to the gas-phase value (see Table S1)

[e] The electronic charge developed on the C_2H_2 molecule is determined by means of the Mulliken population analysis, Q_{MPA}, and the natural population analysis, Q_{NPA}

[f] Because the surfaces are represented by the Pd_{14} and $Pd_{13}Pb$ clusters, some adsorption sites are not symmetric and, therefore, in these cases there are two values of R(C–H) and ∠(C–C–H)

neighborhood poisons their ability to adsorb acetylene. The poisoning effect of Pb can be expressed energetically by E_{ads} and structurally by d, δ_{C-C}, and δ_{C-C-H}. At the structural level, the effect of Pb means that the C_2H_2 molecule is adsorbed higher from the PdPb(100) surface than from the Pd(100) one and the distortion of the adsorbate from its gas-phase geometry is often smaller on PdPb(100).

The reduced activity of PdPb(100) toward the C_2H_2 adsorption originates from the poisoning effect of Pb and thus the monometallic surfaces of Pb should be inactive in the acetylene adsorption process. The absence of the adsorbed acetylene has indeed been reported for the Pb(111) surface [70]. On this basis, it can be deduced that some decrease of the C_2H_2 adsorption ability is expected for all single-crystal Pd–Pb surfaces.

The influence of dopant on surface adsorption properties is often described in terms of ensemble effects and ligand effects [71, 72]. Ensemble effects are associated with the nature of an ensemble of metal atoms with which an adsorbate binds. In other words, they describe changes in surface adsorption properties when the composition of adsorption sites varies. Ligand effects reflect the influence of the surroundings of adsorption sites on surface adsorption properties. These effects are related to the electronic structure of adsorption sites and can be expressed by changes in the d-band centers of surface metal atoms [72, 73].

Out of the investigated variants of the bridge and hollow sites on PdPb(100), the I variant demonstrates the ensemble effect, since in such adsorption sites the Pb atom is one of the atoms with which the C_2H_2 molecule is combined. In the case of the bridge-II and hollow-II sites acetylene is bonded with two Pd atoms and the dopant atom is present in the surroundings of these two Pd atoms. Hence, the bridge-II and hollow-II sites exemplify the ligand effect. As it was mentioned above, the ligand effect is manifested as a shift of the d-band center. The parts of DOS that correspond to the d-bands for Pd(100) and PdPb(100) are shown in Fig. 5. The Pd(100) surface

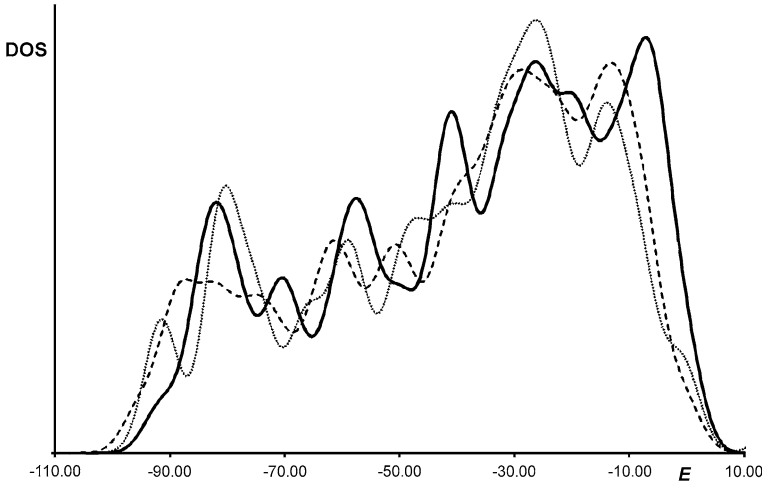

Fig. 5 DOS plots for Pd(100) (*solid line*), PdPb(100) with the surface Pb atom (*dashed line*), and PdPb(100) with the subsurface Pb atom (*dotted line*). The energy, E (kcal/mol), is relative to the Fermi level energy. The values of DOS are given in arbitrary units

exhibits the d-band center for $E = -37.59$ kcal/mol with respect to the Fermi level energy. Bearing this value in mind, the d-band centers of PdPb(100) with the surface Pb atom and with the subsurface Pb atom are shifted down by 3.46 and 2.77 kcal/mol, respectively. Because of the presence of only one Pb atom in the $Pd_{13}Pb$ clusters, the changes in the d-band center for PdPb(100) are very small but they seem to correlate with the adsorption energy of C_2H_2 on PdPb(100). The d-states decrease in energy brings about a weaker interaction between the adsorbate and the surface [72, 73].

The adsorption of the C_2H_2 molecule in the atop-I and atop-II sites deserves a separate discussion. The calculations of the C_2H_2 adsorption in the atop-I and atop-II sites, as well as in the atop one, yield rather large distances from the surfaces, $d > 2.1$ Å, and weak interactions with the surfaces, $E_{ads} > -7$ kcal/mol. The atop-II site exhibits practically the same E_{ads} value as the atop site on Pd(100). Surprisingly, the effect of adsorption in the atop-I site is more exoenergetic than that in the atop site. This is in direct contradiction to the poisoning effect of Pb and thus the E_{ads} value of -6.14 kcal/mol should be treated with caution. It might result from the assumed fixed crystal structure of the metal clusters and the definitive investigation of the C_2H_2 adsorption in the atop, atop-I, and atop-II sites seems to require the incorporation of the surface relaxation into the calculations.

Adsorption of ethylene on Pd(100) and PdPb(100)

Experimental studies performed by Stuve et al. [21, 22] have demonstrated that the C_2H_4 molecule binds with the Pd(100) surface in both di-σ and π configurations at low temperatures. These configurations of C_2H_4 on Pd(100) coexist at 80 K and in this case the $\pi\sigma$ parameter, formulated by Stuve et al. [21, 22] to characterize the bond between ethylene and metallic surfaces, lies midway between π and σ systems. At room temperature, ethylene adsorbs reversibly on Pd(100) [29]. The initial heat of C_2H_4 adsorption on this surface is estimated to be ca. -18 kcal/mol [29].

The energetic, structural, and electronic properties of the C_2H_4 molecule adsorbed in the characteristic sites on the Pd(100) and PdPb(100) surfaces are listed in Table 3. The adsorption energy of the C_2H_4 molecule on Pd(100) is the most exoenergetic in the bridge site, $E_{ads} = -13.93$ kcal/mol. Interestingly, the E_{ads} values for the atop and hollow sites differ only by 1.80 kcal/mol. From the energetic point of view, it would suggest the equivalence of these sites in the C_2H_4 adsorption process, which, in turn, would be in line with the experimental observation concerning the coexistence of the di–σ and π configurations of C_2H_4 [21, 22]. On the other hand, the C_2H_4 molecule in the hollow site lies much closer (by 0.513 Å) to the surface than it does in the atop site. Furthermore, the geometry of ethylene in the hollow site changes markedly, while it is practically unperturbed in the atop site. In the bridge and hollow sites, the C–C bond is elongated (see δ_{C-C} in Table 3) and the C atoms undergo a rehybridization from sp^2 to nearly sp^3 (see δ_{C-C-H_2} in Table 3). The donation of electronic charge from the adsorbate molecule to the surface predominates in the atop and bridge sites, although the Q_{NPA} charges are very small. By contrast, the back-donation transfer dominates in the hollow site.

Table 3 Energetic, structural, and electronic properties of the ethylene molecule adsorbed in the characteristic sites on the Pd(100) and PdPb(100) surfaces

Surface	Site	E_{ads} (kcal/mol)	d (Å)	R(C–C) (Å)	R(C–H) (Å)	∠(C–C–H) (°)	∠(C–C–H_2) (°)	δ_{C-C} (Å)	δ_{C-C-H} (°)	δ_{C-C-H_2} (°)	Q_{MPA} (e)	Q_{NPA} (e)
Pd(100)	Atop	−5.91	2.338	1.362	1.083	121.2	168.5	0.033	0.5	11.5	0.1493	0.0021
	Bridge	−13.93	2.011	1.443	1.088	116.9	142.2	0.114	4.8	37.8	0.2538	0.0658
					1.093	116.2	140.0		5.5	40.0		
	Hollow	−7.71	1.825	1.464	1.089	115.5	136.7	0.135	6.2	43.3	−0.0552	−0.2046
					1.096	114.2	131.9		7.5	48.1		
PdPb(100)	Atop-I	−7.10	2.228	1.379	1.083	120.8	163.3	0.050	0.9	16.7	0.1158	0.1358
					1.083	121.1	163.3		0.6	16.7		
	Bridge-I	−0.69	2.481	1.377	1.084	120.1	170.4	0.048	1.6	9.6	0.1623	0.0562
					1.084	119.9	171.3		1.8	8.7		
	Hollow-I	−1.05	2.423	1.385	1.085	121.6	178.1	0.056	0.1	1.9	0.1281	−0.0983
					1.085	121.6	178.4		0.1	1.6		
	Atop-II	−5.87	2.348	1.359	1.084	121.0	169.7	0.030	0.7	10.3	0.2975	0.2057
					1.085	121.2	170.9		0.5	9.1		
	Bridge-II	−10.77	2.002	1.440	1.090	116.9	142.0	0.111	4.8	38.0	0.3343	0.0880
					1.092	116.6	140.9		5.1	39.1		
	Hollow-II	−5.59	1.957	1.452	1.087	117.5	146.5	0.123	4.2	33.5	0.1077	0.0419
					1.093	116.2	140.7		5.5	39.3		

See the footnotes to Table 2 for further notes

The calculated E_{ads} value in the bridge site on Pd(100) is relatively close to the experimental estimation [29]. The energetic preference of this adsorption site has also been predicted by other theoretical studies [32, 33]. However, the values of −19.4 [32] and −21.5 kcal/mol [33] are more exoenergetic than the result obtained in this work. The structural properties of C_2H_4 in the bridge site from Table 3 are comparable with those from [32, 33]. It should be stressed that there are some discrepancies for ethylene in the atop site. In general, the calculation performed in this work yields a weak interaction, $E_{ads} = -5.91$ kcal/mol, with the large distance between the π-bonded C_2H_4 and the surface, $d = 2.338$ Å. The result of Bernardo and Gomes [32] confirms this weak interaction, $E_{ads} = -7.7$ kcal/mol, but their d value is decreased by 0.3 Å. The smaller d value agrees with that predicted by Ge and Neurock [33], but these authors, in turn, have reported the E_{ads} value equal to −18.8 kcal/mol.

The C_2H_4 adsorption on the PdPb(100) surface remains energetically favorable for all sites, although the exoenergetic effects are very small for the bridge-I and hollow-I sites. Among the considered sites containing or neighboring with the Pb atom, the bridge-II one is designated as the most favorable site for the C_2H_4 adsorption. The E_{ads} values of −0.69 and −1.05 kcal/mol in the bridge-I and hollow-I sites, respectively, are very close to zero and, within the framework of the computational approach applied in this work, they seem to be beyond the accuracy limit in order to be able to detect unambiguously any attractive interaction between the adsorbate and the surface. Thus, the lack of the attractive interaction in these sites can be assumed at the qualitative level. Such an assumption is supported by the structural properties: the δ_{C-C}, δ_{C-C-H}, and δ_{C-C-H_2} parameters indicate practically the gas-phase geometry of C_2H_4 and the heights from the surface are greater than 2.4 Å. By contrast, the binding of C_2H_4 in the bridge-II and hollow-II sites is undisputed. The C–C bond length increases and the C atoms exhibit a rehybridization from sp^2 to nearly sp^3. The rehybridization gives rise to the elevation of the H atoms above the molecule plane (see δ_{C-C-H_2} in Table 3). The C_2H_4 adsorption in the atop-II site is energetically slightly more favorable than that in the hollow-II site. For the former the distance between the Pb atom and the adsorbate is larger, which makes the negative effect of Pb weaker. The donation of electronic charge from C_2H_4 to the surface predominates when the Pb atom is located in the subsurface layer.

Both variants of the bridge and hollow sites on the PdPb(100) surface exhibit less exoenergetic E_{ads} values than the bridge and hollow sites on Pd(100). These less exoenergetic values of E_{ads} can be explained in terms of the ensemble effect (for the bridge-I and hollow-I sites) and the ligand effect (for the bridge-II and hollow-II sites). The ligand effect on the C_2H_4 adsorption is associated with the shifts of the d-band center for the doped surfaces (see Fig. 5). In the case of three adsorption sites with the subsurface Pb atom, the changes in E_{ads} are rather small, less than 3.2 kcal/mol compared to the E_{ads} values on Pd(100). The structural properties of the C_2H_4 molecule adsorbed in the atop-II and bridge-II sites are very similar to those of ethylene in the atop and bridge sites on Pd(100). The effect of the subsurface Pb atom is more pronounced for the hollow-II site that

binds the C_2H_4 molecule at larger distance from the surface and with smaller distortion of its geometry than the hollow site on Pd(100) does. The presence of the surface Pb atom in the bridge-I and hollow-I sites brings about larger decreases of the adsorption exoenergeticity than those observed for the sites with the subsurface Pb atom. It is particularly evident for the bridge-I site which is

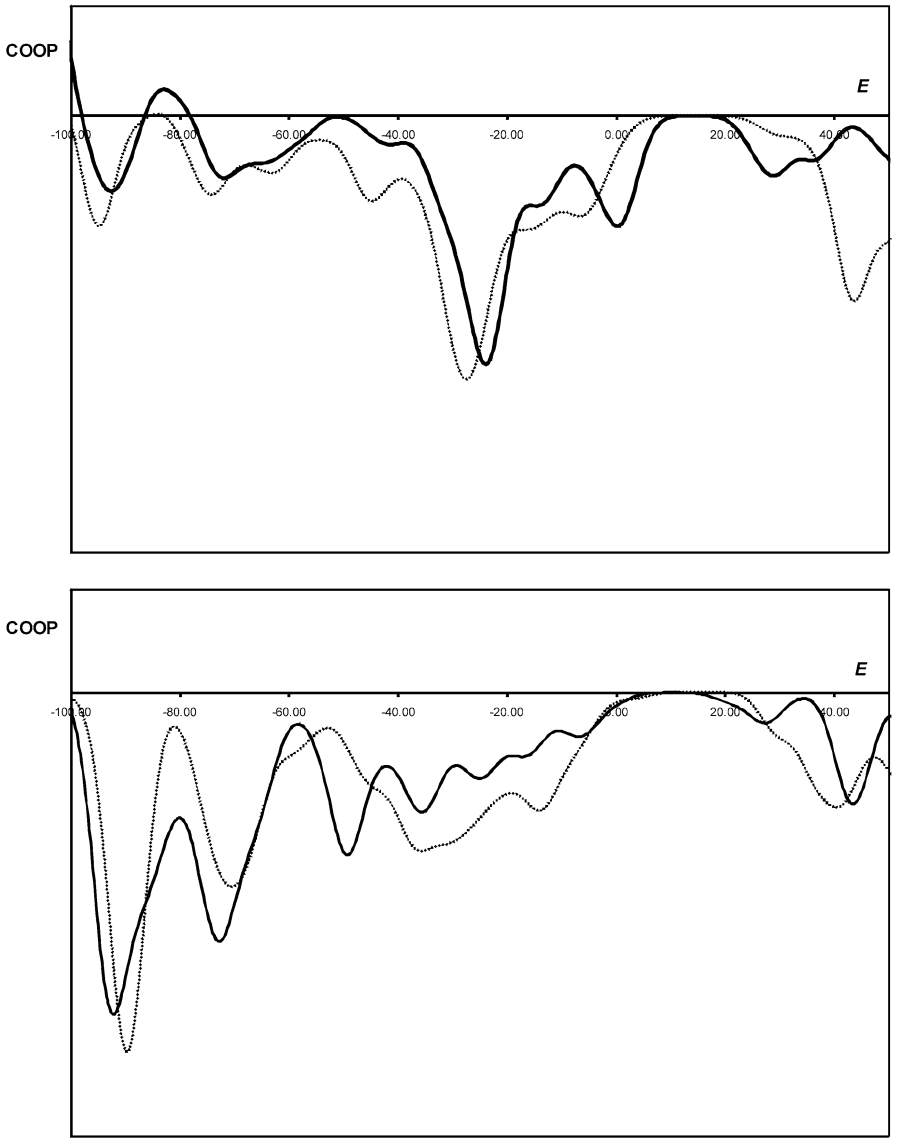

Fig. 6 Top panel: COOP plots for C_2H_2 adsorbed in the bridge site on Pd(100) (*solid line*) and in the bridge-II site on PdPb(100) (*dotted line*). Bottom panel: COOP plots for C_2H_4 adsorbed in the bridge site on Pd(100) (*solid line*) and in the bridge-II site on PdPb(100) (*dotted line*). The energy, *E* (kcal/mol), is relative to the Fermi level energy. The values of COOP are given in arbitrary units

deactivated by the surface Pb atom. The atop-I site demonstrates an exceptional behavior resulting in the smaller *d* value, together with a slight strengthening of the interaction. The same was observed for the C_2H_2 adsorption and it was discussed in the previous subsection.

For a given variant of the bridge or hollow site, Pb decreases exoenergetic effect more strongly for the C_2H_2 adsorption than for the C_2H_4 adsorption. The same has been detected for the PdPb(111) surface by García-Mota et al. [42] who have reported the decreases of 15.45 and 11.99 kcal/mol for acetylene and ethylene, respectively. On the basis of the results obtained by Sheth et al. [38] for PdAg (111), it can be expected that the adsorption energies for acetylene are also more sensitive to changes in the alloy composition (i.e., the increasing amount of Pb) than those for ethylene. The more significant decrease of the exoenergetic effect of the C_2H_2 adsorption obviously does not mean that the C_2H_4 becomes the most favorable. On the contrary, the adsorption of C_2H_4 on PdPb(100) exhibits less exoenergetic effect than that of the C_2H_2 adsorption for a given variant of the bridge or hollow site. The poisoning effect of Pb is sufficient to reduce, or even deactivate, the ability of the surface to adsorb ethylene, while acetylene can still be bound relatively strongly. Thus, from the thermodynamic point of view [2], the better selectivity can be achieved for PdPb(100) compared to Pd(100).

The more pronounced effect of the Pb dopant on the C_2H_2 adsorption in comparison to the C_2H_4 adsorption can also be characterized by means of the COOP between the adsorbate and the surface. The plots of COOP for C_2H_2 and C_2H_4 adsorbed in the bridge and bridge-II sites are shown in Fig. 6. For each adsorbate the shape of the COOP in the bridge-II site on PdPb(100) does not differ significantly from that in the bridge site on Pd(100). However, the antibonding combinations (that is, those beneath the energy axis in Fig. 6) of the adsorbate orbitals with the surface orbitals are slightly shifted below the Fermi level energy when the dopant is present. This shift seems to be more evident for the C_2H_2 adsorption and, therefore, it suggests the greater change in E_{ads}.

Conclusions

In this work, the interaction between some simple molecules (such as H_2, C_2H_2, and C_2H_4) and Pd–Pb catalysts was investigated using the B3LYP hybrid density functional. The reaction paths for the H_2 molecule reacting with the PdPb dimer are reported for the singlet and triplet spin states. As for the C_2H_2 and C_2H_4 molecules, their adsorption in a few characteristic sites on the Pd(100) surface doped with Pb was studied in order to determine some energetic, structural, and electronic properties of these adsorbates.

From the presented results of the calculations, the following conclusions can be drawn:

1. Only the Pd end of the bimetallic dimer captures the H_2 molecule in its molecular form with a small exoenergetic effect. The dissociation of H_2 on PdPb requires activation.

2. On the Pd(100) surface doped with Pb, among the considered adsorption sites containing or neighboring with a single Pb atom, the hollow site with the subsurface Pb atom (i.e., the hollow-II variant) turns out to be energetically preferred for the C_2H_2 adsorption, whereas the bridge site with the subsurface Pb atom in its immediate proximity (i.e., the bridge-II variant) is the most favorable for the C_2H_4 adsorption.
3. The presence of Pb in the PdPb dimer and in the PdPb(100) surface reduces the activity of such catalysts toward the adsorption and dissociation of H_2 and toward the adsorption of C_2H_2 and C_2H_4. From the thermodynamic point of view, it assists in improving the selectivity of the Pd–Pb catalysts.

Acknowledgments The CYFRONET AGH Academic Computer Center is acknowledged for access to the Baribal supercomputer (Computational Grant No. MEiN/SGI3700/UŁódzki/078/2006).

References

1. Malleron J-L, Fiaud J-C, Legros J-Y (1997) Handbook of palladium-catalyzed organic reactions. Academic Press, New York
2. Molnár Á, Sárkány A, Varga M (2001) J Mol Catal A Chem 173:185
3. King AO, Larsen RD, Negishi E (2002) In: Negishi E (ed) Handbook of organopalladium chemistry. Wiley, New York, p 2719
4. Brown MW, Penlidis A, Sullivan G (1991) Can J Chem Eng 69:152
5. Jin Y, Datye AK, Rightor E, Gulotty R, Waterman W, Smith M, Holbrook M, Maj J, Blackson J (2001) J Catal 203:292
6. Teschner D, Borsodi J, Wootsch A, Révay Z, Hävecker M, Knop-Gericke A, Jackson SD, Schlögl R (2008) Science 320:86
7. Teschner D, Révay Z, Borsodi J, Hävecker M, Knop-Gericke A, Schlögl R, Milroy D, Jackson SD, Torres D, Sautet P (2008) Angew Chem Int Ed 47:9274
8. Seriani N, Mittendorfer F, Kresse G (2010) J Chem Phys 132:024711
9. Vogel W (2011) J Phys Chem C 115:1506
10. Coq B, Figueras F (2001) J Mol Catal A Chem 173:117
11. Nørskov JK, Bligaard T, Rossmeisl J, Christensen CH (2009) Nat Chem 1:37
12. Thanh CN, Didillon B, Sarrazin P, Cameron C (2000) US patent, 6054409
13. Choudhary TV, Sivadinarayana C, Datye AK, Kumar D, Goodman DW (2003) Catal Lett 81:1
14. Aduriz HR, Bodnariuk P, Coq B, Figueras F (1991) J Catal 129:47
15. Choi SH, Lee JS (2000) J Catal 193:176
16. Palczewska W, Jabłoński A, Kaszkur Z (1984) J Mol Catal 25:307
17. Sandoval VH, Girola CE (1996) Appl Catal A Gen 148:81
18. Kesmodel LL (1983) J Chem Phys 79:4646
19. Gentle TM, Muetterties EL (1983) J Phys Chem 87:2469
20. Tysoe WT, Nyberg GL, Lambert RM (1984) J Phys Chem 88:1960
21. Stuve EM, Madix RJ (1985) J Phys Chem 89:105
22. Stuve EM, Madic RJ, Brundle CR (1985) Surf Sci 152–153:535
23. Rucker TG, Logan MA, Gentle TM, Muetterties EL, Somorjai GA (1986) J Phys Chem 90:2703
24. Wang LP, Tysoe WT, Ormerod RM, Lambert RM, Hoffmann H, Zaera F (1990) J Phys Chem 94:4326

25. Heitzinger JM, Gebhard SC, Koel BE (1993) J Phys Chem 97:5327
26. Dunphy JC, Rose M, Behler S, Ogletree DF, Salmeron M, Sautet P (1998) Phys Rev B 57:R12705
27. Janssens TVW, Völkening S, Zambelli T, Wintterlin J (1998) J Phys Chem B 102:6521
28. Sandell A, Beutler A, Jaworowski A, Wiklund M, Heister K, Nyholm R, Andersen JN (1998) Surf Sci 415:411
29. Vattuone L, Yeo YY, Kose R, King DA (2000) Surf Sci 447:1
30. Sellers H (1990) J Phys Chem 94:8329
31. Neurock M, Van Santen RA (2000) J Phys Chem B 104:11127
32. Bernardo CGPM, Gomes JANF (2001) J Mol Struct THEOCHEM 542:263
33. Ge Q, Neurock M (2002) Chem Phys Lett 358:377
34. Bertani V, Cavallotti C, Masi M, Carrà S (2003) J Mol Catal A Chem 204–205:771
35. Medlin JW, Allendorf MD (2003) J Phys Chem B 107:217
36. Mei D, Hansen EW, Neurock M (2003) J Phys Chem B 107:798
37. Mittendorfer F, Thomazeau C, Raybaud P, Toulhoat H (2003) J Phys Chem B 107:12287
38. Sheth PA, Neurock M, Smith CM (2005) J Phys Chem B 109:12449
39. Andersin J, Lopez N, Honkala K (2009) J Phys Chem C 113:8278
40. Lindlar H (1952) Helv Chem Acta 35:446
41. Ferullo RM, Touroude R, Castellani NJ (1997) Surf Rev Lett 4:621
42. García-Mota M, Gómez-Díaz J, Novell-Leruth G, Vargas-Fuentes C, Bellarosa L, Bridier B, Pérez-Ramírez J, López N (2011) Theor Chem Acc 128:663
43. Studt F, Abild-Pedersen F, Bligaard T, Sørensen RZ, Christensen CH, Nørskov JK (2008) Angew Chem Int Ed 47:9299
44. Hill JM, Shen J, Watwe RM, Dumesic JA (2000) Langmuir 16:2213
45. Frisch MJ et al (2004) Gaussian 03, revision E.01. Gaussian Inc, Wallingford
46. Becke AD (1993) J Chem Phys 98:5648
47. Slater JC (1974) Quantum theory of molecular and solids. Vol. 4: the self-consistent field for molecular and solids. McGraw-Hill, New York
48. Becke AD (1988) Phys Rev A 38:3098
49. Vosko SH, Wilk L, Nusair M (1980) Can J Phys 58:1200
50. Lee C, Yang W, Parr RG (1988) Phys Rev B 37:785
51. Wang MY, Liu XJ, Meng J, Wu ZJ (2007) J Mol Struct THEOCHEM 804:47
52. Hay PJ, Wadt WR (1985) J Chem Phys 82:299
53. Roy LE, Hay PJ, Martin RL (2008) J Chem Theory Comput 4:1029
54. McLean AD, Chandler GS (1980) J Chem Phys 72:5639
55. Fukui K (1981) Acc Chem Res 14:363
56. Bartczak WM, Stawowska J (2004) Struct Chem 15:447
57. Messmer RP, Knudson SK, Johnson KH, Diamond JB, Yang CY (1976) Phys Rev B 13:1396
58. Kertesz M, Hoffmann R (1984) J Am Chem Soc 106:3453
59. O'Boyle NM, Tenderholt AL, Langner KM (2008) J Comput Chem 29:839
60. Huber KP, Herzberg G (1979) Constants of diatomic molecules. Van Nostrand Reinhold, New York
61. Pershina V, Anton J, Fricke B (2007) J Chem Phys 127:134310
62. Ciccioli A, Balducci G, Gigli G, Perring L, Bussy F (2000) Intermetallics 8:195
63. Boys SF, Bernardi F (1970) Mol Phys 19:553
64. Matczak P (2011) Reac Kinet Mech Cat 102:1
65. Alikhani ME, Minot C (2003) J Phys Chem A 107:5352
66. Dewar MJS (1951) Bull Soc Chim Fr 18:C79
67. Chatt J, Duncanson LA (1953) J Chem Soc 2939
68. Mulliken RS (1955) J Chem Phys 23:1833
69. Glendening ED, Reed AE, Carpenter JE, Weinhold F (2004) Gaussian NBO Version 3.1
70. Fuhrmann D, Wacker D, Weiss K, Hermann K, Witko M, Ch Wöll (1998) J Chem Phys 108:2651
71. Lam YL, Criado J, Boudart M (1997) Nouv J Chim 1:461
72. Liu P, Nørskov JK (2001) Phys Chem Chem Phys 3:3814
73. Mavrikakis M, Hammer B, Nørskov JK (1998) Phys Rev Lett 81:2819